

# Fluid inclusion modification by H<sub>2</sub>O and D<sub>2</sub>O diffusion: the influence of inclusion depth, size, and shape in re-equilibration experiments

Gerald Doppler · Ronald J. Bakker ·  
Miriam Baumgartner

Received: 2 August 2012 / Accepted: 25 January 2013 / Published online: 14 February 2013  
© Springer-Verlag Berlin Heidelberg 2013

**Abstract** The mobility of H<sub>2</sub>O and D<sub>2</sub>O by diffusion through quartz is illustrated with H<sub>2</sub>O-rich fluid inclusions synthesized at 600 °C and 337 MPa, within the  $\alpha$ -quartz stability field. Inclusions are re-equilibrated at the same experimental conditions within a pure D<sub>2</sub>O fluid environment. Consequently, a gradient in volatile fugacities is the only driving force for diffusion, in the absence of pressure gradients and deformation processes. Up to 100 individual inclusions are analyzed in each experiment before and after re-equilibration by microscopic investigation, microthermometry, and Raman spectroscopy. Changes in fluid inclusion composition are obtained from the ice-melting temperatures, and density changes are obtained from total homogenization temperatures. After 1-day re-equilibration, inclusions already contain up to 11 mol % D<sub>2</sub>O. A maximum concentration of 63 mol % D<sub>2</sub>O is obtained after 40-day re-equilibration. D<sub>2</sub>O concentration profiles in quartz are determined from the concentration in inclusions as a function of their distance to the quartz surface. These profiles illustrate that deep inclusions contain less D<sub>2</sub>O than shallow inclusions. At equal depths, a variety of D<sub>2</sub>O concentration is observed as a function of fluid inclusion size: Small inclusions are stronger effected compared with large inclusions. A series of 19-day re-equilibration

experiments are performed at 300, 400, 500, and 600 °C (at 337 MPa), at the same conditions as the original synthesis. The threshold temperature of diffusion is estimated around 450 °C at 337 MPa, because D<sub>2</sub>O is not detected in inclusions from re-equilibration experiments at 300 and 400 °C, whereas maximally 26 mol % D<sub>2</sub>O is detected at 500 °C. Our study indicates that the isotopic composition of natural fluid inclusions may be easily modified by re-equilibration processes, according to the experimental conditions at 600 °C and 337 MPa.

**Keywords** Fluid inclusions · Quartz · Diffusion · Re-equilibration · Experimental study · Hydrogen isotopes · D<sub>2</sub>O · H<sub>2</sub>O

## Introduction

Most of the nominally anhydrous minerals within the Earth's crust and mantle can incorporate considerable and measurable amounts of hydrogen (e.g. Keppler and Smyth 2006). The major incorporated species is assumed to be hydroxyl, that is, OH<sup>−</sup> (e.g. Keppler and Smyth 2006). Molecular H<sub>2</sub>O is generally concentrated in specific nano- to micrometer-sized isolated cavities within single crystals, but H<sub>2</sub>O molecules can also be present at interstitial lattice positions. Cavities that exceed diameters of about 1  $\mu$ m are usually known as fluid inclusions, which can be analyzed by optical means (e.g. Shepherd et al. 1985). Nominally anhydrous quartz is a common host mineral of fluid inclusions, and the entrapped fluids are used in a widespread field of geological investigations (see Roedder 1984 and references therein). Knowledge of the properties of this fluid may contribute to reconstructions of pressure–temperature–time (*P–T–t*) histories of rock units in the Earth's

Communicated by J. Touret.

**Electronic supplementary material** The online version of this article (doi:10.1007/s00410-013-0857-6) contains supplementary material, which is available to authorized users.

G. Doppler (✉) · R. J. Bakker · M. Baumgartner  
Chair of Resource Mineralogy, Department of Applied  
Geological Sciences and Geophysics, University of Leoben,  
Leoben, Austria  
e-mail: gerald.doppler@unileoben.ac.at

crust and may contribute to understanding fluid–rock interactions. The interpretation of paleo-fluids in inclusions is among other assumptions based on the hypothesis that the entrapped inclusions remain their density and composition after entrapment. Fluid inclusion research is generally based on a closed-system assumption within nominal anhydrous minerals. However, there is experimental evidence that entrapped inclusions do not always behave as closed systems (e.g. Sterner and Bodnar 1989; Bakker and Jansen 1990, 1994; Diamond et al. 2010). Detailed studies on the distribution and properties of fluid inclusions in natural samples also suggest post-entrapment modifications (e.g. Audétat and Günther 1999; Ayllón et al. 2003). The experimental studies on modification of fluid inclusions in quartz are not conclusive, because the impact of individual parameters, such as temperature, gradients in concentration, gradients in pressure, fluid-quartz interactions, host mineral phase transitions (e.g.  $\alpha$ – $\beta$  quartz), and deformation, on modification processes are not yet fully unraveled (e.g. Bakker and Diamond 2003). Most experimental studies do not separate the influence of these individual parameters on modification processes. For example, fluid inclusions in experiments that have mimicked nearly isothermal decompression are effected by gradients in fluid composition, gradients in fluid pressure (i.e. in fluid densities), and inclusion wall deformation processes at variable hydrothermal pressures and slightly decreasing temperatures. Any modification of fluid properties in these inclusions results from applying all of these variables at once. In order to estimate the effect of individual parameters, it is essential to accumulate more experimental data of post-entrapment modifications of fluid inclusions by performing systematic experiments in which only one variable is adjusted, whereas the others remain constant.

The present study describes major parameters that play a significant role in H<sub>2</sub>O and D<sub>2</sub>O diffusion experiments. The mobility of hydrogen isotopes in nominally anhydrous crystals is of major importance for the interpretation of constraints on the origin of parental fluids from which ore-forming minerals have grown (e.g. Giuliani et al. 1997). In this context, the determination of isotopic composition of fluid inclusions has recently increased in importance (e.g. Wilkinson 2001; Dublyanski and Spötl 2010). Any modification of the  $\delta$ D composition of natural fluid inclusions due to re-equilibration processes will result in inaccurate fluid source identification, especially in magmatic and metamorphic environments. There are no studies available that document in detail the efficiency of D<sub>2</sub>O–H<sub>2</sub>O diffusion through quartz that may affect  $\delta$ D values of fluid inclusions.

In the present study, only hydrothermal activity of H<sub>2</sub>O as the entrapped species and D<sub>2</sub>O as the external fluid phase at constant  $P$ – $T$  conditions of 337 MPa and 300, 400,

500, and 600 °C leads to the diffusional driving force regarding to the gradient of the chemical potential. Each presented experiment in this study was exclusively performed under hydrothermal experimental conditions without any experimental stress component. In order to avoid any changes of the initially entrapped inclusions during the start and the end of the experiments, loading and unloading the autoclave (pressure vessel) is performed at constant fluid density conditions (isochorically) exclusively in the  $\alpha$ -quartz stability field. Previous re-equilibration experiments have been carried out in a widespread stability field of quartz, but probably without respect to the different crystallographic modifications of  $\alpha$ -quartz and  $\beta$ -quartz (e.g. Sterner and Bodnar 1989; Vityk and Bodnar 1995). Contrary to assumptions of previous work (e.g. Sterner et al. 1995), non-decrepitative changes of inclusion properties are directly related to the combination of (1) depth within the crystal; (2) inclusions size; (3) temperature; and (4) time. The experiments demonstrate the major factors that cause the mobility of water through quartz under hydrothermal experimental conditions and, therefore, the experimental alteration of natural fluid inclusions as they are currently performed by the authors (Baumgartner et al. 2011; Bakker et al. 2012). The newly acquired data of the compositional changes result in new diffusion models and diffusion constants of H<sub>2</sub>O and D<sub>2</sub>O in quartz.

## Experimental procedure

The hydrothermal laboratory at the University of Leoben is specially designed for the synthesis of fluid inclusions. There are 10 Nimonic IOS/René 41 autoclaves (Ni–Cr alloy) in a vertical position that are installed in a cold-seal system (see Kerrick 1987). The pressure medium is Argon and may reach values up to 1 GPa hydrothermal pressure. The external oven temperatures are maximally 700 °C. Temperatures are directly measured at the samples within the autoclaves with an internal thermocouple. Temperature is controlled by a computerized operating system during the experiment and is measured with an uncertainty of 0.1 °C. The pressure is monitored with pressure transducers, which are calibrated up to 700 MPa with a Heise dial gauge (accuracy is 0.015 % of reading). Both temperature and pressure are continuously logged.

The experimental work is designed to synthesize fluid inclusions in quartz of known  $V_m$ – $x$  properties (i.e. molar volume and composition, respectively), morphological properties, and positions within the crystal. The quartz samples with initially synthesized pure H<sub>2</sub>O fluid inclusions are exposed to a pure D<sub>2</sub>O environment during the re-equilibration experiment at the same temperature and pressure conditions. Consequently, gradients in temperature

and pressure or deformation conditions are not present during experimentation. Both, synthesis and re-equilibration experiments, are carried out under hydrothermal conditions. Due to a compositional gradient, that is, fugacity gradients of  $\text{H}_2\text{O}$  and  $\text{D}_2\text{O}$  between synthetic fluid inclusions and the external fluid phase during the re-equilibration experiments, diffusion of the two species through the quartz crystal is provoked.

#### Fluid inclusion synthesis

Inclusion-free natural Brazilian quartz crystals are used as starting material. Rods are drilled in specific crystallographic orientations of the quartz crystal, with an approximate length of 1 cm and diameter of 2.75 mm. The direction of drilling is parallel to the *c*-axis of the quartz crystal to minimize the influence of birefringence of the laser light in subsequent Raman spectroscopic analyses of fluid inclusions (Baumgartner and Bakker 2009). The quartz rods are partially cracked by a thermal shock after heating to 400 °C. A cracked quartz rod and a certain amount of ultra-pure water are loaded within an Au-capsule, that is, arc-welded on both sides to prevent any interaction with the autoclaves and the pressure medium Argon at experimental conditions. The synthesis is performed by healing fractures according to the method of Bodnar and Sterner (1987).

The *P*–*T* conditions of the synthesis experiments are given in Table 1. All experiments are performed at 337 MPa and various temperatures, that is, 300, 400, 500, and 600 °C, within the  $\alpha$ -quartz stability field (Hosieni et al. 1985). The selected conditions are purely arbitrary and represent crustal conditions at about 10 km depth and variable temperatures, as it may occur in different geothermal gradients. The experimental setup stabilizes the synthesis conditions within 2 °C and 3 MPa (Table 1), and fluid inclusions are synthesized within 19 days. The experiments are loaded and unloaded according to specific isochores of the fluid trapped in the newly formed inclusions (see Appendix A in ESM) to prevent stress conditions that may cause cracking of inclusions due to internal fluid over- or under-pressures. This can only be achieved by the use of internal thermo-couples.

After the initial synthesis of aqueous fluid inclusions, the quartz rods are cut into disks with a thickness of approximately 0.5 mm. Subsequently, the disks are polished on both sides for microscopic, microthermometric, and Raman spectroscopic investigations. A relatively large number of fluid inclusions (up to 100, see Table 1) of each disk are analyzed to achieve statistical distributions of a variety in parameters such as sizes, shapes, and distances to the crystal surface, that is, depth within the quartz crystal (see Appendix B in ESM).

#### Re-equilibration of fluid inclusions

After various analyses of the initially synthesized fluid inclusions, the same quartz disks are subsequently used for re-equilibration experiments. The relatively fragile sample disks are placed in between two quartz spacers to prevent any damage by capsule deformation during re-equilibration. Instead of ultra-pure water, pure  $\text{D}_2\text{O}$  is added to the gold capsule in re-equilibration experiments. Loading as well as unloading of the pressure vessels is carried out again according to specific isochores such that the pressure in the initial fluid inclusions does not differ from the external pressure medium. The experimental *P*–*T* conditions of re-equilibration experiments are illustrated in Table 1 and do not differ from the original synthesis conditions. The experimental run-times vary from 1, 5, 19 to 40 days, and re-equilibration conditions are stabilized within 2 °C and 3 MPa (Table 1). After the re-equilibration experiments, composition ( $\text{H}_2\text{O}$ – $\text{D}_2\text{O}$  mixture), density, and morphology are compared with the initially synthesized fluid inclusions.

#### Analytical methods

Morphological properties of each fluid inclusion are characterized by the total area and the perimeter by tracing digitally around the outside edges of the fluid inclusions at room temperature according to Bakker and Diamond (2006). The volumetric properties of individual phases (liquid/vapor ratio) are difficult to obtain; therefore, area fractions of the vapor bubble ( $a_{\text{vap}}$ ) of each fluid inclusion have been digitally measured from two-dimensional images by tracing the outside edge of the total inclusion and by the outside rim of the vapor bubble at room temperature. The distance of fluid inclusions to the crystal surface is measured with an ordinary microscope table that is adjustable in the *z*-direction (Olympus BX60).

Homogenization and melting temperatures of the entrapped fluids are measured by using the LINKAM MDS 600 and LINKAM THMSG 600 heating–freezing stages, which are calibrated with synthetic fluid inclusions at –56.6 °C (melting of  $\text{CO}_2$ ), 0.0 °C (melting of  $\text{H}_2\text{O}$ ), and 374.0 °C (critical density of  $\text{H}_2\text{O}$ ). The precision of measurements is  $\pm 0.1$  °C around 0 °C and about  $\pm 0.3$  °C in the range of 300–400 °C. The reproducibility of all measurements is within  $\pm 0.1$  °C.

The presence of  $\text{H}_2\text{O}$  and  $\text{D}_2\text{O}$  in fluid inclusions is detected by an ISA JobinYvon LABRAM confocal Raman spectrometer, using a frequency-doubled 120 mW Nd-YAG laser with an excitation wavelength of 532.2 nm. Raman spectra of both  $\text{H}_2\text{O}$  and  $\text{D}_2\text{O}$  are broad bands within a range of wavenumbers that do not interfere (Fig. 1), 2,900–3,800 and 2,100–2,800  $\text{cm}^{-1}$ , respectively

**Table 1** Experimental conditions

a	b	c	d	e	f	g	h	i	j	k	l	m
Syntheses												
GMR002c	338.5	±2.8	600.2	±0.2	176.9	±1.8	24.97	–	–	–	19	100
GMR004a	336.0	±1.6	601.4	±2.0	176.0	±2.0	25.06	–	–	–	19	96
GMR004b	336.0	±1.6	601.4	±2.0	176.0	±2.0	25.06	–	–	–	19	100
GMR004c	336.0	±1.6	601.4	±2.0	176.0	±2.0	25.06	–	–	–	19	77
GMR006a	337.4	±1.5	300.3	±0.6	28.9	±0.3	19.06	–	–	–	19	15
GMR007a	337.6	±1.0	400.7	±0.6	69.0	±0.5	20.66	–	–	–	19	47
GMR008a	334.9	±2.0	500.1	±0.4	119.7	±1.0	22.67	–	–	–	19	98
Re-equil.												
R002c	336.9	±0.6	599.8	±0.3	175.7	±0.6	25.00	176.17	±0.55	24.91	5	94
R004a	337.3	±2.0	599.5	±1.6	175.8	±2.1	24.98	176.26	±2.14	24.89	19	90
R004b	335.9	±2.5	600.1	±0.9	175.3	±1.9	25.03	175.75	±1.96	24.94	1	100
R004c	336.1	±1.7	600.3	±0.4	175.4	±1.2	25.03	175.95	±1.25	24.94	40	33
R006a	336.7	±1.0	299.7	±0.8	28.6	±0.4	19.06	27.88	±0.36	19.09	19	12
R007a	336.8	±1.1	399.9	±0.8	68.3	±0.7	20.65	67.60	±0.68	20.76	19	30
R008a	337.2	±0.6	499.5	±0.8	120.3	±0.7	22.62	120.31	±0.65	22.68	19	91

(a) Number and type of experiment (GMR = synthesis; R = re-equilibration)

(b) Pressure (MPa)

(c) Pressure variation (MPa)

(d) Temperature (°C)

(e) Temperature variation (°C)

(f) H<sub>2</sub>O fugacity (MPa; Haar et al. 1984; software from Bakker 2003; <http://fluids.unileoben.ac.at>)(g) H<sub>2</sub>O fugacity variation (MPa)(h) H<sub>2</sub>O molar volume (cm<sup>3</sup> mol<sup>−1</sup>; Haar et al. 1984; software from Bakker 2003)(i) D<sub>2</sub>O fugacity (MPa; Hill et al. 1982; software from Bakker, <http://fluids.unileoben.ac.at>)(j) D<sub>2</sub>O fugacity variation (MPa)(k) D<sub>2</sub>O molar volume (cm<sup>3</sup> mol<sup>−1</sup>; Hill et al. 1982; software from Bakker, <http://fluids.unileoben.ac.at>)

(l) Run-time (days)

(m) Number of measured fluid inclusions

(see also Rull 2002). Therefore, the relative amounts of D<sub>2</sub>O and H<sub>2</sub>O in fluid inclusions can be directly obtained by comparing their relative band areas in a spectrograph. Standard solutions of known variable H<sub>2</sub>O/D<sub>2</sub>O ratios were measured by Baumgartner et al. (2011) and reveal a simple relationship between ratio and area fractions (Eq. 1)

$$x_{\text{rel}}(\text{D}_2\text{O}) = \frac{a_{\text{D}_2\text{O}}}{a_{\text{D}_2\text{O}} + a_{\text{H}_2\text{O}}} \quad (1)$$

where  $x_{\text{rel}}$  is the relation mole fraction of D<sub>2</sub>O in binary D<sub>2</sub>O–H<sub>2</sub>O mixtures and  $a$  is the band area.

The Raman cross-sections of H<sub>2</sub>O and D<sub>2</sub>O do not need to be considered in this purely empirical relationship. The D<sub>2</sub>O content of re-equilibrated synthetic fluid inclusion is directly calculated with this equation. The D<sub>2</sub>O composition is compared with melting temperatures of the D<sub>2</sub>O/H<sub>2</sub>O mixture, and significant different melting temperatures  $T_m(\text{SV} \rightarrow \text{LV})$  of pure H<sub>2</sub>O (0.0 °C) and pure D<sub>2</sub>O

(+3.8 °C) can be used to determine relative amounts of H<sub>2</sub>O and D<sub>2</sub>O from intermediate melting temperatures. Consequently, these temperature changes can be directly related to relative band areas in Raman spectra (Eq. 1), resulting in a simple equation to calculate H<sub>2</sub>O/D<sub>2</sub>O mole fractions from  $T_m$  values (Eq. 2)

$$x_{\text{rel}}(\text{D}_2\text{O}) = \frac{T_m(\bar{f}_i)}{T_m^0(\text{D}_2\text{O}) - T_m^0(\text{H}_2\text{O})} \quad (2)$$

where  $T_m$  is melting temperature in °C,  $\bar{f}_i$  is the solution in a specific fluid inclusion. The superscript 0 indicates the pure phase.

The properties of H<sub>2</sub>O and D<sub>2</sub>O fluids are calculated with equations of state, Haar et al. (1984) and Hill et al. (1982), respectively, that are available in the software package *FLUIDS* provided by Bakker (2003, and <http://fluids.unileoben.ac.at>).

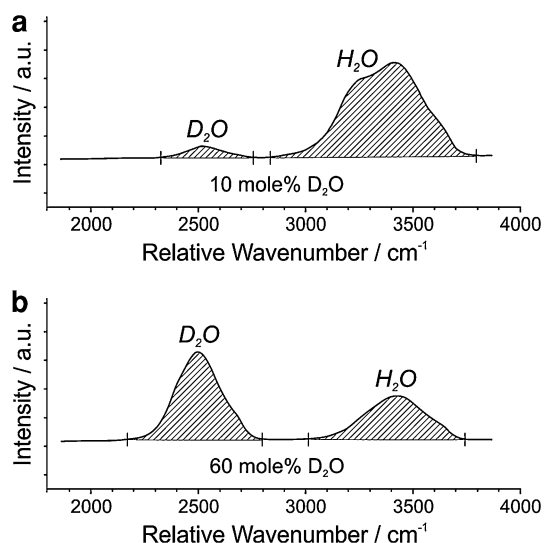


**Fig. 1** Raman spectra of fluid inclusions (originally pure H<sub>2</sub>O) after a re-equilibration experiment. Inclusion with 10 mol % D<sub>2</sub>O (**a**) and inclusion with 60 mol % D<sub>2</sub>O (**b**). The peak area is directly related to the relative amount of the fluid species

### Fugacity, molar volume, and homogenization temperatures of H<sub>2</sub>O and D<sub>2</sub>O

Fugacity and molar volume calculations of pure H<sub>2</sub>O in the initial synthesis are given in Table 1 (column *f* and *h*). Experiments *GMR002c* and *GMR004a, b*, and *c* have been performed at 600 °C and 337 MPa which corresponds to a molar volume of 25 cm<sup>3</sup> mol<sup>−1</sup> and a fugacity of 175.8 MPa. Additional three syntheses have been carried out at lower temperatures and at approximately the same pressure. Synthesis *GMR008a* has been carried out at 500 °C which corresponds to a molar volume of 22.63 cm<sup>3</sup> mol<sup>−1</sup> and a fugacity of 120.5 MPa. Experiment *GMR007a* has been performed at 400 °C with a molar volume of 20.65 cm<sup>3</sup> mol<sup>−1</sup> and a fugacity of 68.42 MPa. The lowest temperature synthesis *GMR006a* has been performed at 300 °C which corresponds to a molar volume of 19.06 cm<sup>3</sup> mol<sup>−1</sup> and a fugacity of 28.74 MPa. The fugacity of H<sub>2</sub>O in the external fluid in re-equilibration experiments is reduced to 0 MPa, due to the absence of H<sub>2</sub>O in the capsule. H<sub>2</sub>O fugacity within fluid inclusions and the D<sub>2</sub>O fugacity in the capsule fluid during re-equilibration are illustrated in Table 1 (column *f* and *i*, respectively). Comparison of both fugacities indicates the similarities of both fluids at equal *P–T* conditions.

The equations of state for H<sub>2</sub>O (Haar et al. 1984) and D<sub>2</sub>O (Hill et al. 1982) are used to calculate isochores and homogenization temperatures (*T<sub>h</sub>*) of fluid inclusions, from the experimental *P–T* conditions. At 600 °C and 337 MPa (experiments *GMR002c*; *GMR004a, b, c*; *R002c*; *R004a, b, c*), pure H<sub>2</sub>O fluid inclusions homogenize in the liquid

phase at 295.6 °C, whereas pure D<sub>2</sub>O inclusions homogenize at 294.6 °C. The minor difference between these *T<sub>h</sub>* values indicates that the isochores in both systems nearly coincide. At 500 °C and 337 MPa, the *T<sub>h</sub>* values are 252.0 °C and 253.4 °C for H<sub>2</sub>O and D<sub>2</sub>O, respectively. The maximum difference in *T<sub>h</sub>* values is obtained from 400 °C and 337 MPa experimental conditions: 193.4 °C for H<sub>2</sub>O and 197.3 °C for D<sub>2</sub>O. *T<sub>h</sub>* values of 117.5 °C and 119.3 °C are calculated for H<sub>2</sub>O and D<sub>2</sub>O, respectively, from experimental conditions of 300 °C and 337 MPa.

### Diffusion of H<sub>2</sub>O and D<sub>2</sub>O

The gradient in chemical potential of H<sub>2</sub>O and D<sub>2</sub>O between inclusions and the external capsule fluid is directly related to the fugacity gradient, an important parameter which effects bulk diffusion (e.g. Crank 1975). Relative free communication of fluid species between inclusions and external fluid through a quartz crystal would more or less instantaneously result in equalization of fugacities, according to the published theories of diffusion (see Bakker 2009). Extremely low solubility of H<sub>2</sub>O in quartz is a major barrier for relative fast diffusion. It is expected that the imposed gradients in H<sub>2</sub>O and D<sub>2</sub>O fugacity in our experiments result in measurable changes in fluid inclusion density and composition. Bulk diffusion of fluid species in minerals is also controlled by temperature and time, which both may have a major impact on concentration profiles of fluid species in the quartz crystal. The influences of these parameters are investigated in a series of experiments in this study. The length of diffusion path (i.e. distance of fluid inclusions to the crystal surface) and fluid inclusion size are other parameters, which define the amount of inclusion alteration due to diffusion processes. In theory, diffusional changes in fluid inclusion composition are not related to changes in fluid inclusion morphology.

The boundary conditions of the diffusion experiments in this study are defined by the geometry of the quartz sample, that is, a short cylinder, where H<sub>2</sub>O and D<sub>2</sub>O are able to enter the quartz in all directions: along the top or bottom plane and along the side (three-dimensional diffusion). The external fluid in the capsule is regarded as an infinite source and is wetting all sides of the quartz sample during the experimentation.

### Experimental results

Up to 100 fluid inclusions of each experiment are photographed for identification purposes and for achieving the morphological properties, mainly the size and the inclusion shape. Each inclusion is analyzed by microthermometry and Raman spectroscopic methods. Each individual fluid



inclusion is analyzed before and after re-equilibration (see Appendix B).

### Initial experiments

The shapes of the originally synthesized fluid inclusions after 19 days of experimentation show a large variety (Fig. 2) according to the definition of Bakker and Diamond (2006). At 600 °C, about 90 % of all fluid inclusions are defined by a regular shape, varying between elongated and equant. However, the variation in inclusion shape is also large between the different samples that are used in the initial synthesis (c.f. Fig. 2a, b, and c). Fluid inclusions are formed in the open volume limited by the micro-crack walls that were generated in quartz by thermal shock before experimentation; therefore, the size and shape of these cracks are important factors that determine this variability. At 500 °C (Fig. 2d), 85 % of all fluid inclusions have regular shapes. This percentage decreases further at lower experimental temperatures: 67 % at 400 °C (Fig. 2e) and only 60 % at 300 °C (Fig. 2f).

The measured fluid inclusions of all synthesis experiments (*GMR002c*; *GMR004a, b, c*; *GMR006a*; *GMR007a*; and *GMR008a*) reveal similar freezing and melting behavior (see Appendix B): Ice-melting temperatures vary between +0.1 and −0.1 °C in all measurements, which reflects the accuracy of microthermometry. The experiments at 600 °C and 337 MPa reveal average  $T_h$  of 293.2, 293.1, 292.7, and 293.8 °C (all within the liquid phase) for *GMR002c*, *GMR004a, b*, and *c*, respectively (Table 2, Fig. 3a). The variability in these temperatures is about  $\pm 5$  °C. The experiments at 300, 400, and 500 °C reveal  $T_h$ 's of 130.9, 200.8, and 254.3 °C for *GMR006a*, *GMR007a*, and *GMR008a*, respectively (Table 2).

The liquid–vapor ratio, that is, the volume fraction of the vapor phase in individual fluid inclusions at room temperatures and the measured homogenization temperatures, is compared in Fig. 3b. Both parameters are measures of the molar volume (or density) of fluid inclusions. According to Bakker and Diamond (2006), the area fraction ( $a_{\text{vap}}$ ) of the vapor phase in two-dimensional images of regular-shaped fluid inclusions can be used as a measure of volume fraction. The  $T_h$  histogram (Fig. 3a) illustrates a relative narrow range with a mode (maximum frequency) between 293 and 294 °C and has passed the Shapiro–Wilk normality test (Shapiro and Wilk 1965); wherefore, a normal distribution of the  $T_h$  values can be recognized. The  $a_{\text{vap}}$  histogram (Fig. 3b) has a relative broad spread, between 15 and 40 %, with a mode between 20 and 25 %. The gray-shaded bar (26–27 %) in Fig. 3b indicates  $a_{\text{vap}}$  values that are calculated directly with homogenization temperatures (mode values) of this synthesis. The variability in shape of fluid inclusions results in a broad spread

of  $a_{\text{vap}}$  values, and the statistical mode appears at slightly lower values than the calculated values from  $T_h$ . This observation is conform to the study of Bakker and Diamond (2006), who illustrated that irregular-shaped fluid inclusions always have smaller numbers on area fractions of vapor bubbles in two-dimensional images than on volume fractions. It also illustrates that  $T_h$  measurements result in more accurate molar volume estimations than area fraction measurements, if a reliable equation of state is available for the fluid system in inclusions that is able to transform these temperatures into molar volumes.

### Morphological modifications of fluid inclusions after re-equilibration

Each sample in this study is re-equilibrated at the same pressure and temperature conditions as the initial synthesis to avoid any stress component in the crystal lattice surrounding the fluid inclusions. After re-equilibration, some of the inclusions show notable morphology changes (Figs. 2, 4). Originally synthesized irregular and elongated inclusions tend to become more equant and regular during re-equilibration process. Originally equant and regular inclusions tend to become negative crystal-shaped. The extend of morphological changes is dependent on the re-equilibration time. At 600 °C, after 5 days of re-equilibration (*R002c*, Figs. 2a, 4b), only relatively small changes in the shape distribution field can be detected and most fluid inclusions are regular, either elongated or equant. More notable changes occur after a re-equilibration time of 19 days (*R004a*, Figs. 2b, 4c). Elongation and irregularity of fluid inclusions are clearly reduced toward more regular and equant shapes. The 40-day re-equilibration experiment (*R004c*, Figs. 2c, 4d) reveals the most regular fluid inclusions. After recrystallization of the inclusion walls in this re-equilibration experiment, the entire assemblage is defined as regular inclusions, with a maximum elongation of about 6 (major/minor ratio of best-fit ellipse, see Bakker and Diamond 2006).

The change in fluid inclusion shape after 19 days of experimentation is compared at a variety of temperatures: 300, 400, 500, and 600 °C (Figs. 2b, d–f, 4c, e–g). The amount of change of individual inclusions decreases to lower experimental temperatures. At 600 °C, the shape distribution field is clearly reduced after re-equilibration, whereas at 500 °C, the reduction is relatively less, and at 400 °C, there is no change in the shape distribution field (c.f. Fig. 2b, d, e). In contrast, at 300 °C (Fig. 2f), the shape distribution displays a relatively large reduction after re-equilibration. The low number of analyzed fluid inclusions (15) does not represent an extensive statistical examination and may cause a distortion of the shape distribution field.

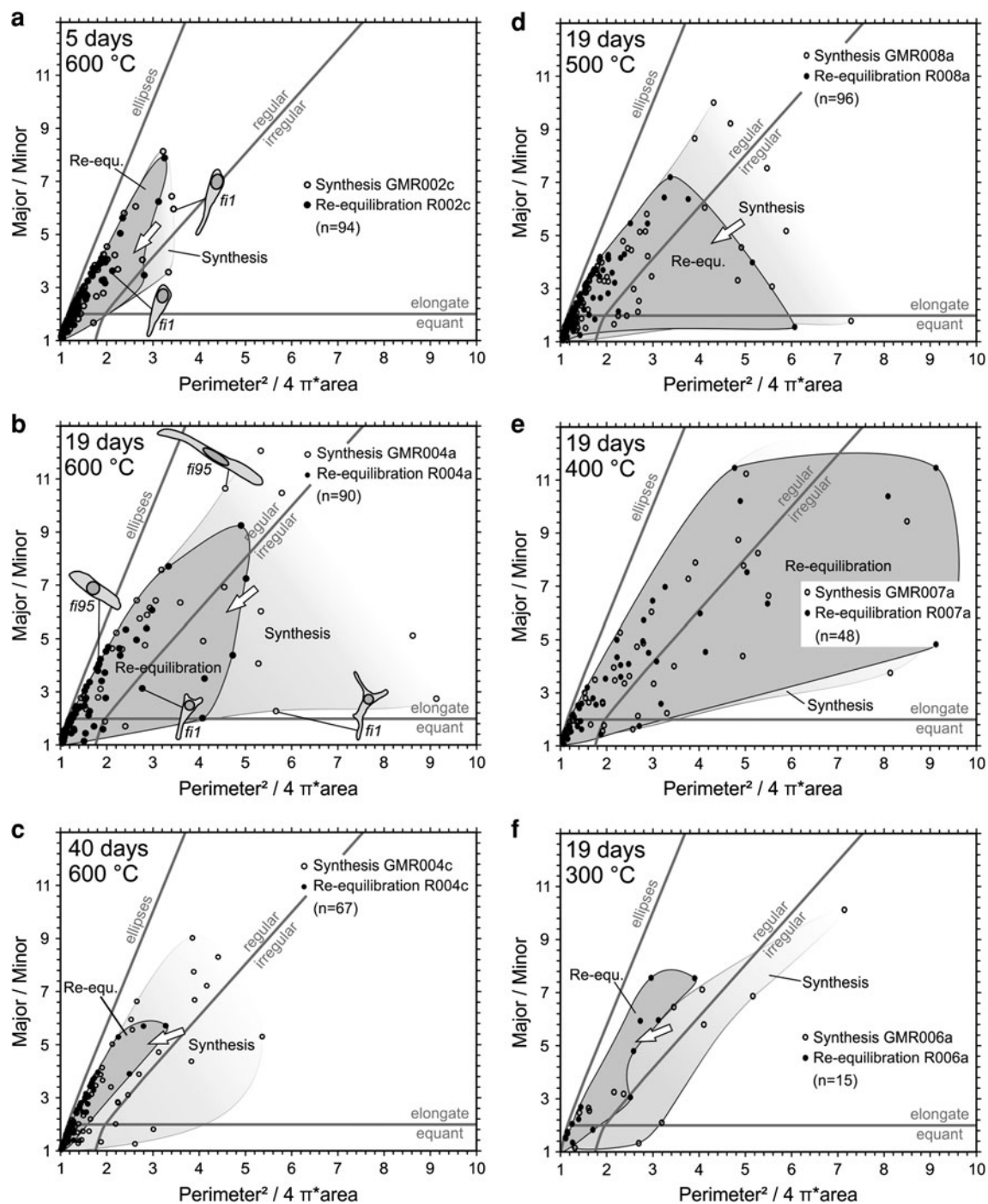


**Fig. 2** Fluid inclusion shape classification diagrams of the experiments. The open circles are measurements after the original synthesis; the filled circles represent the same inclusions after re-equilibration. The run-times of the synthesis experiments are 19 days. Inclusion shapes at experimental conditions at 600 °C and 337 MPa are illustrated after 5 days (**a**), 19 days (**b**) and 40 days (**c**) of re-equilibration. Nineteen-day experimental run-times (re-equilibration

experiments) are compared at different temperatures in **b** 600 °C, **d** 500 °C, **e** 400 °C, and **f** 300 °C. The open arrows indicate a general shift in fluid inclusion shape changes of the re-equilibrations. *fi1* in **a** illustrates the change in shape of an individual fluid inclusion at 600 °C, 337 MPa after 5 days re-equilibration. A much larger shift of individual *fi*'s is illustrated in **b**; *fi1* and *fi95*

Changes in total volume are not identified within two-dimension images of all analyzed fluid inclusions and can be excluded because of the absence of any stress or

pressure gradients around inclusions. The dimensions of all fluid inclusions do not seem to have changed after re-equilibration.

**Table 2** Homogenization temperatures from initial experiments and re-equilibration experiments, melting temperatures with corresponding D<sub>2</sub>O content after re-equilibration

a	b	c	d	e	f	g	h	i	j
GMR002c	293.2	+4.6	−1.8	R002c	295.7	+4.9	−1.5	1.8	47
GMR004a	293.1	+2.5	−4.6	R004a	293.5	+2.4	−4.2	2.4	63
GMR004b	292.7	+3.1	−2.2	R004b	293.1	+3.1	−2.2	0.4	11
GMR004c	293.8	+3.0	−3.4	R004c	293.2	+1.9	−1.8	2.4	63
GMR006a	130.9	+5.9	−4.9	R006a	130.4	+6.1	−4.7	0.0	0
GMR007a	200.8	+4.2	−2.4	R007a	201.3	+2.3	−1.8	0.0	0
GMR008a	254.3	+5.1	−4.9	R008a	254.6	+4.6	−4.2	1.0	26

(a) Synthesis experiment

(b) Mean  $T_h$  (homogenization temperature) initial synthesis (°C)(c) Maximum  $T_h$ —mean  $T_h$  initial synthesis (°C)(d) Mean  $T_h$ —minimum  $T_h$  initial synthesis (°C)

(e) Corresponding re-equilibration experiment

(f) Mean  $T_h$  re-equilibration (°C)(g) Maximum  $T_h$ —mean  $T_h$  re-equilibration (°C)(h) Mean  $T_h$ —minimum  $T_h$  re-equilibration (°C)(i) Maximum  $T_m$  (melting temperature) re-equilibration (°C)(j) Maximum mole % D<sub>2</sub>O

### Density and compositional changes of fluid inclusions after re-equilibration

Noticeable changes in H<sub>2</sub>O–D<sub>2</sub>O composition of initially synthesized inclusions are obtained in all re-equilibration experiments at 600 and 500 °C, whereas changes are not detected in experiments at 400 and 300 °C (all experimental data are presented in the Appendix B). Changes in composition of fluid inclusions are already detected after a relatively short re-equilibration time (e.g. 1 day, *R004b*). The changes are measured in terms of ice-melting temperatures and homogenization temperatures (Figs. 5, 6, 7).

At 600 °C (Fig. 5), four re-equilibration experiments were performed in 1 day (*R004b*), 5 days (*R002c*), 19 days (*R004a*), and 40 days (*R004c*). Fluid inclusions that have completely exchanged their H<sub>2</sub>O content with D<sub>2</sub>O at a constant total volume at experimental conditions must end up in the point at  $T_m(\text{ice}) = +3.8$  °C and  $\Delta T_h = -1.3$  °C in Fig. 5. At an equal exchange rate of one molecule H<sub>2</sub>O diffusing outward and one molecule D<sub>2</sub>O diffusing inward, all possible pairs of  $T_m$  and  $T_h$  must be positioned on the inclined dashed line in Fig. 5. Minor amounts of D<sub>2</sub>O (maximal 11 mol %) are already detected after 1 day of re-equilibration (Fig. 5a), as deduced from an increase of maximally 0.4 °C of  $T_m(\text{ice})$ . A decrease in bulk density is evidenced by an increase in  $T_h$ , with maximally +1.3 °C, which illustrates the loss of H<sub>2</sub>O. These results prove that the gain of D<sub>2</sub>O is a slower process than the loss of H<sub>2</sub>O after 1 day. This unexpected shift becomes even more prominent after 5 days of experimentation (Fig. 5b):

$T_m(\text{ice})$  reaches maximum values of +1.8 °C (47 mol % D<sub>2</sub>O), illustrating diffusion of D<sub>2</sub>O into fluid inclusions; and  $T_h$  values shift maximally to +4.9 °C, illustrating a loss in density, or a faster outward diffusion of H<sub>2</sub>O than inward diffusion of D<sub>2</sub>O. Inclusions with a low D<sub>2</sub>O content, that is, lower  $T_m(\text{ice})$ , reveal a higher shift in  $T_h$  than inclusions with a high D<sub>2</sub>O content. After 19 days of re-equilibration (Fig. 5c), D<sub>2</sub>O contents have reached a maximum value of 63 mol %, corresponding to  $T_m(\text{ice})$  of +2.4 °C. In contrast to the 5-day re-equilibration experiments,  $T_h$ 's have a much lower positive shift and become even negative for inclusions with higher D<sub>2</sub>O contents. The temperature changes are approaching the equal exchange conditions, as continuous D<sub>2</sub>O diffusion is slowly drawing level with the faster H<sub>2</sub>O diffusion. After 40 days of re-equilibration (Fig. 5d), all microthermometric measurements are positioned on the mixing line between the two end members: starting conditions (0.0 °C) and the end point (+3.8, −1.3 °C). These four re-equilibration experiments at 600 °C illustrate that fluid inclusion modifications are not uniform, and a whole range of D<sub>2</sub>O contents and density changes are detected for each experiment. Likely, the controlling factors for these changes are diffusion processes through quartz and depend on the size and distance to the grain boundary of individual inclusions. These re-equilibration experiments also illustrate that data obtained in relative short experimental run-times (less than 19 days) may lead to incorrect interpretations of processes, because changes in homogenization temperatures occur in the opposite direction.



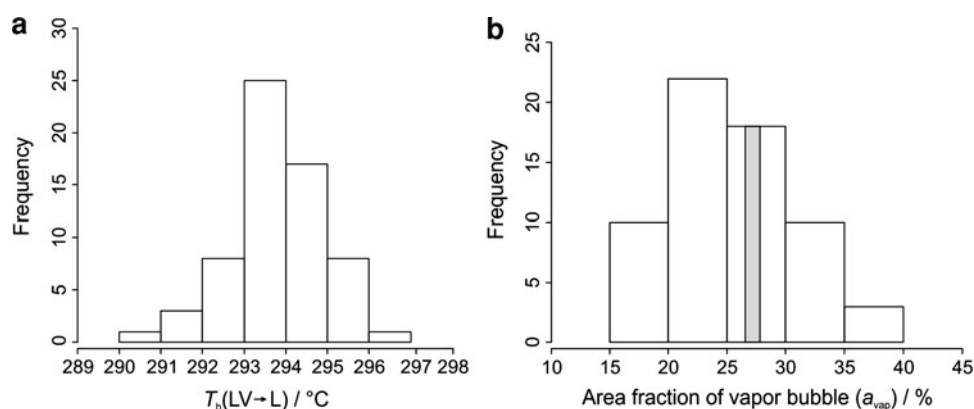


**Fig. 3** The histograms ( $n = 63$ ) are exemplarily illustrated based on the data of the experiment *GMR004c*. **a** The histogram shows the  $T_h$  range from 290.4 to 296.8 °C with a median of 293.7 °C and a mode of 293–294 °C. **b** Illustration of the  $a_{vap}$  with the broad spread

between 15 and 40 % and the mode of 20–25 %. The gray-shaded bar shows the calculated  $a_{vap}$  value based on the  $T_h$  values of this synthesis illustrated in **a**. Detailed fluid inclusion properties are summarized in Table 2

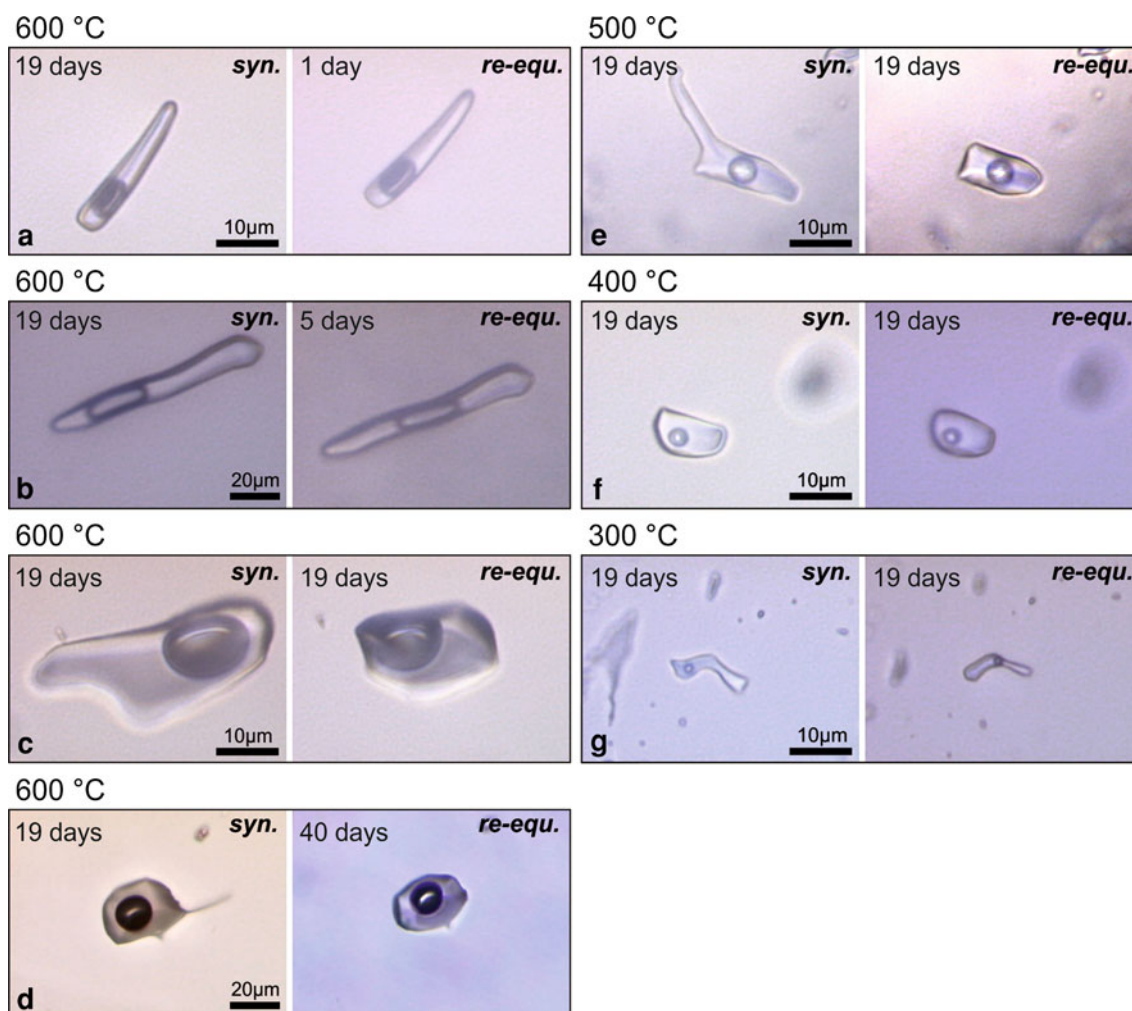


**Fig. 4** Photomicrographs of the same inclusions before (syn. = synthesized) and after (re-equ. = re-equilibration) the re-equilibration experiment at 600 °C (**a–d**), 500 °C (**e**), 400 °C (**f**), and 300 °C (**g**). Different run-times are illustrated at 600 °C: (**a**) 1 day; (**b**) 5 days; (**c**) 19 days; and (**d**) 40 days. The synthesis and re-equilibration

experiments illustrated are **a** *GMR004b–R004b*, **b** *GMR002c–R002c*, **c** *GMR004a–R004a*, and **d** *GMR004c–R004c*. Experiments with equal re-equilibration times and different temperatures are shown in **e** *GMR008a–R008a*, **f** *GMR007a–R007a*, and **g** *GMR006a–R006a*

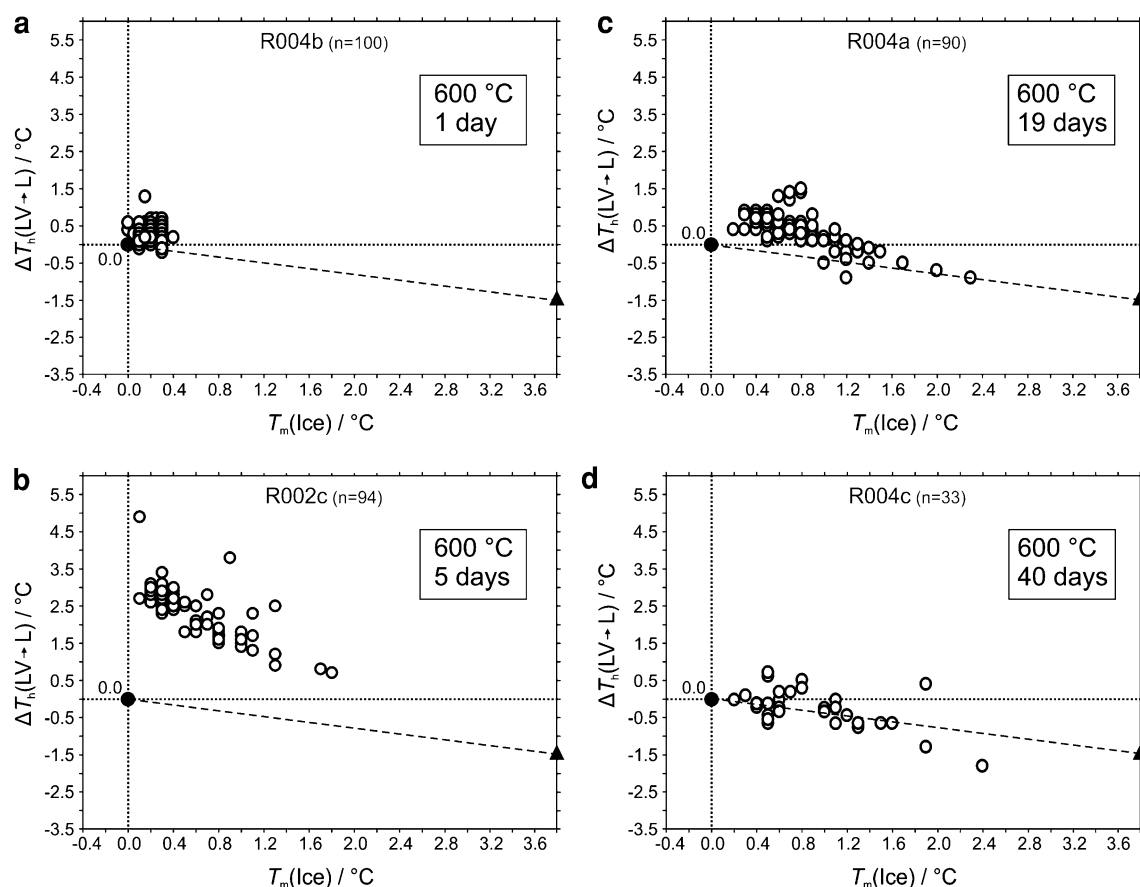


**Fig. 5** Ice-melting temperatures and change in homogenization temperatures of re-equilibrated fluid inclusions at 600 °C and 337 MPa. **a** After 1 day of re-equilibration; **b** after 5 days of re-equilibration; **c** 19 days of re-equilibration; and **d** after 40 days of

experimentation.  $\Delta T_h$  of  $-1.3$  °C indicates the maximum negative shift of homogenization temperature with a fluid inclusion composition of 100 mol %  $D_2O$ ,  $T_m(ice) = +3.8$  °C, respectively. (see text for further detail)

The re-equilibration experiment at 500 °C with a run-time of 19 days at 337 MPa (Fig. 6) shifts  $T_m(ice)$  to a maximum value of  $+1.0$  °C, which corresponds to 26 mol %  $D_2O$ . The  $T_h$  increase to positive values with a maximum of  $+1.6$  °C. The changes in microthermometric temperatures are much less compared with the experiments at 600 °C and 19 days run-time (c.f. Fig. 5c). At equal exchange conditions, all pairs of  $T_m$  and  $\Delta T_h$  must be positioned on the mixing line between the starting point (0.0 °C) and the endpoint at  $T_m(ice) = +3.8$  °C,  $\Delta T_h = +1.4$  °C, which corresponds to a complete replacement of  $H_2O$  by  $D_2O$  in fluid inclusions (inclined dashed line in Fig. 6). Similar to the experiment at 600 °C,  $\Delta T_h$  changes to slightly higher values than expected from the mixing line, which illustrates again that  $H_2O$  is faster diffusing out of fluid inclusions than  $D_2O$  is diffusing in.

In respect to the temperature-depended diffusion phenomena, four experiments have been performed with the same run-times (19 days) at 337 MPa and at different temperatures: 300, 400, 500, and 600 °C (Fig. 7).

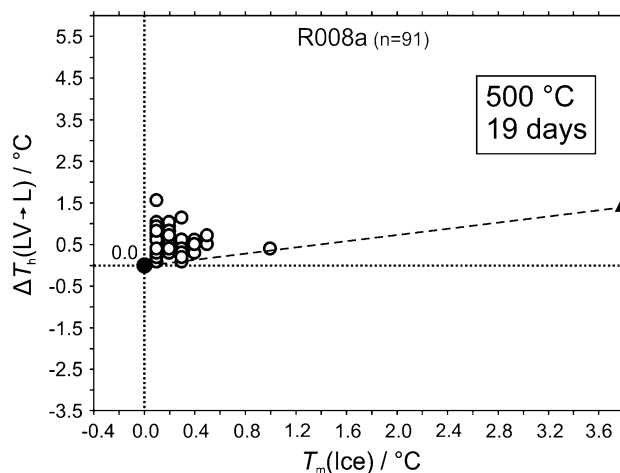


**Fig. 6** Ice-melting temperatures and change in homogenization temperatures of re-equilibrated fluid inclusions at 500 °C and 337 MPa after 19 days of experimentation.  $\Delta T_h$  of  $+1.6$  °C indicates the maximum positive shift of homogenization temperature with a fluid inclusion composition of 100 mol %  $D_2O$ ,  $T_m(ice) = +3.8$  °C, respectively. (see text for further detail)

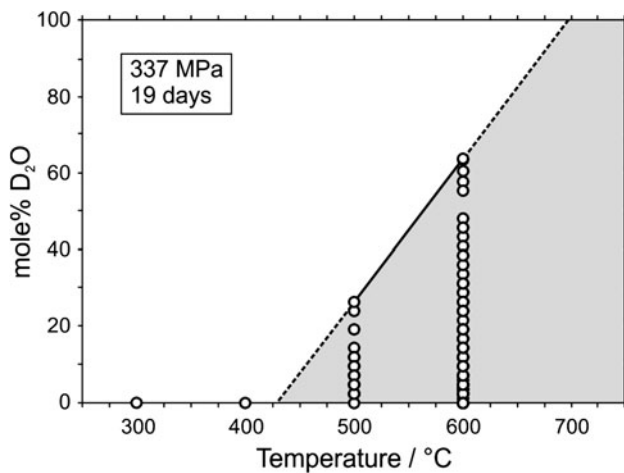


**Fig. 7** D<sub>2</sub>O contents (mole %) of fluid inclusions after the re-equilibration processes at 337 MPa and 19 days of experimentation time at 300, 400, 500, and 600 °C. The inclined solid line illustrates the maximum D<sub>2</sub>O concentration in fluid inclusions. Extrapolation to lower temperatures (dashed line) indicates a threshold temperature of diffusion around 450 °C, whereas a complete exchange of D<sub>2</sub>O is reached around 650 °C after 19 days of experimentation at 337 MPa. The gray area illustrates the range of D<sub>2</sub>O concentration that is observed in the present experiments

Considerably, changes in composition (up to 26 mol % D<sub>2</sub>O) of the initially entrapped fluid are detected after re-equilibration at 500 °C, whereas at 600 °C, inclusions may contain up to 63 mol % D<sub>2</sub>O. Compositional changes in fluid inclusions are not detected in the experiments at 300 and 400 °C. Consequently, it is expected that the threshold temperature of fluid inclusion re-equilibration is around 450 °C, whereas complete adjustment to external condition is obtained at temperatures above 650 °C.

#### Concentration profiles: depth and size relation

As the position of each investigated fluid inclusion within the quartz crystal is measured (see Appendix B), the accordant composition can be plotted in concentration profiles that are related to the depth, considering the distance to the crystal surface (i.e. top or bottom of the short quartz cylinder). Data of the experiment at 600 °C (Fig. 8) illustrate that at specific depths variations in D<sub>2</sub>O concentration can be measured in terms of  $T_m(\text{ice})$ , and that an envelope can be constructed which indicates the limit of maximum concentration. With increasing distance to the crystal surface, the maximum concentrations of D<sub>2</sub>O in re-equilibrated fluid inclusions are decreasing. After 1 day of re-equilibration at 600 °C (Fig. 8a), deep inclusions reveal the same concentration of D<sub>2</sub>O as shallow inclusions, and a relatively flat maximum concentration profile can be drawn, with the maximum  $T_m(\text{ice})$  at +0.4 °C (10 mol % D<sub>2</sub>O). Concerning the longer run-time experiments at 600 °C (5, 19, and 40 days in Fig. 8b–d), a shift of the

respective envelope is recorded. After longer run-times, the shallow inclusions reach maximum compositional change (approaching a pure D<sub>2</sub>O content) earlier than deep inclusions. For example, inclusions at about 225 μm depth reach a maximum D<sub>2</sub>O concentration (39 mol % D<sub>2</sub>O) corresponding to  $T_m(\text{ice}) = +1.5$  °C after 40 days (Fig. 8d), whereas inclusions at about 110 μm depth reach this concentration already after 19 days (Fig. 8c). Inclusions at 100 μm depth display a continuous increase in maximum  $T_m(\text{ice})$  values from +0.4, +1.0, +1.6 to +2.4 °C after 1, 5, 19, and 40 days, respectively. It should be noted that at specific depths, the D<sub>2</sub>O concentrations vary between a maximum value, which defines the envelope, and a minimum value. This minimum D<sub>2</sub>O concentration is only slowly shifting to higher values at higher experimentation run-times (c.f. Fig. 8b, c). The range of values indicates that there is another important parameter that defines the concentration of D<sub>2</sub>O in re-equilibrated fluid inclusions, in addition to the path-length of diffusion.

The envelopes of maximum D<sub>2</sub>O concentration are summarized in the concentration profile in Fig. 9a to illustrate the development of the profile by direct comparison of different experimental run-times. In addition, Fig. 9b illustrates the temperature effect for equal run-time experiments (19 days). The envelope at 500 °C reaches much lower  $T_m(\text{ice})$  values at a specific depth than the envelope at 600 °C. Changes in composition are not detected at 300 and 400 °C at any depth (Fig. 7).

The second parameter that influences the concentration profile is the size of fluid inclusions. The size of inclusions at approximately equal depth is plotted against their  $T_m(\text{ice})$  value for the experiment at 600 °C and 337 MPa in Fig. 10. Variable concentrations at equal depth as shown in Fig. 8c for 19 days run-time are reflecting the size of fluid inclusions: Small inclusions have a higher D<sub>2</sub>O content than large inclusions (Fig. 10a). This is clearly illustrated by fluid inclusions at approximately 75 μm depth (interval 69–80 μm) and 25 μm depth (interval 19–29 μm) after the re-equilibration experiment (Fig. 10a). Inclusions at ±25 μm depth show a less variable D<sub>2</sub>O content, that is, smaller inclusions are only slightly enriched in D<sub>2</sub>O compared with larger inclusions, but have much higher D<sub>2</sub>O concentrations than inclusions at 75 μm depth. The smallest inclusions have the highest D<sub>2</sub>O concentrations and are similar in both depth intervals, which indicate that these inclusions re-equilibrate in a similar way independent from the distance to the surface. After 40 days of re-equilibration (Fig. 10b), the D<sub>2</sub>O content at all depths is similar and mainly dependent on the size of the fluid inclusions. The inclusions at approximately 25 μm depth (interval 20–29 μm) have a larger variation in D<sub>2</sub>O content than the inclusions from the 19 days experiment and reach much higher values (up to 63 mol % D<sub>2</sub>O). Inclusions at

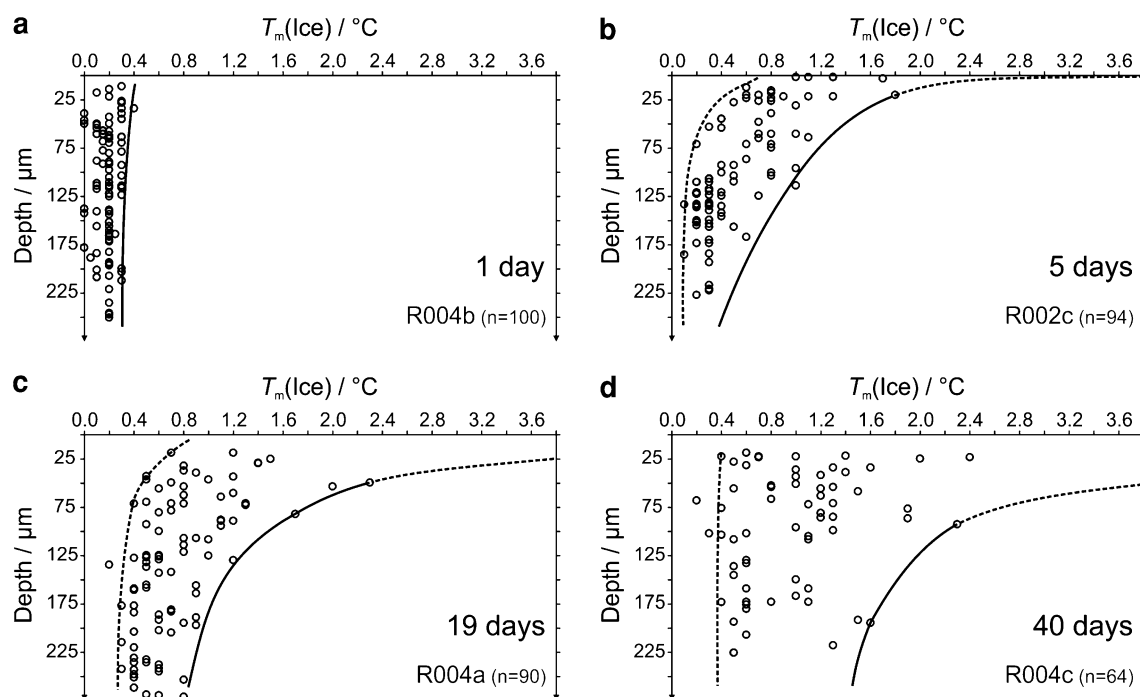


**Fig. 8** Concentration profiles in terms of  $T_m(\text{ice})$  values after re-equilibration of fluid inclusions at 600 °C and 337 MPa after **a** re-equilibration time of 1 day (R004b); **b** re-equilibration time of 5 days (R002c); **c** re-equilibration time of 19 days (R004a); and **d** re-

equilibration time of 40 days (R004c). The dashed and solid curves indicate the boundary of maximum and minimum melting temperatures. Each experiment shows the effect of depth, that is, distance of fluid inclusion to the crystal surface

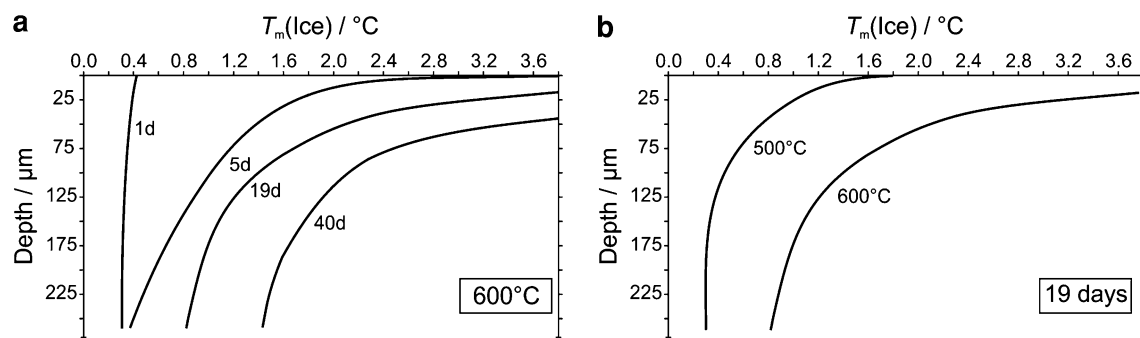


**Fig. 9** Maximum concentration profiles (solid lines) in terms of  $T_m(\text{ice})$  values at 600 °C and 337 MPa; **a** with variable experimental run-times (1, 5, 19, and 40 days). The concentration profiles are

shifting to higher  $T_m(\text{ice})$  values with progressing experimentation time. **b** a comparison of maximum concentration profiles at 600 and 500 °C with 19-day experimental run-time

100  $\mu\text{m}$  depth (interval 96–105  $\mu\text{m}$ ) in the 40-day experiment (Fig. 10b) have similar concentrations as inclusion from the 19-day experiment (c.f. 75  $\mu\text{m}$  depth, Fig. 10a), however, within a much larger range of inclusion sizes.

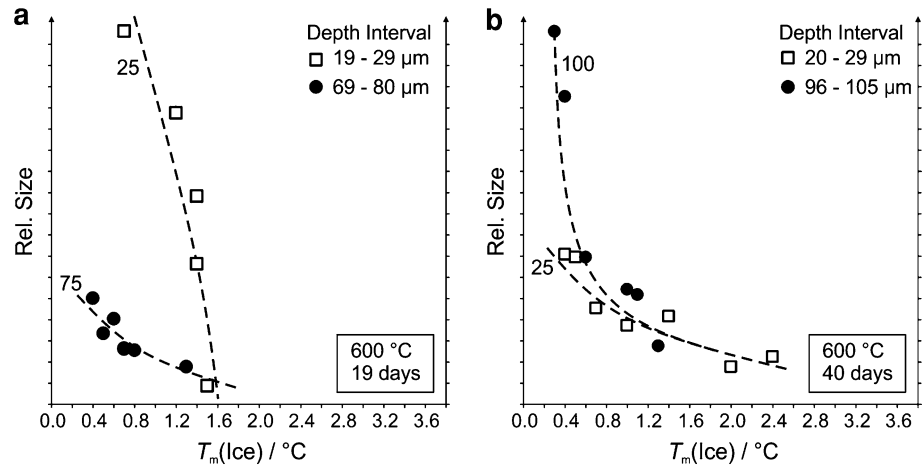
## Discussion

### Diffusion model

The mobility of  $\text{H}_2\text{O}$  and  $\text{D}_2\text{O}$  through quartz crystals at constant temperature and pressure conditions is visualized

at about 337 MPa and 500–600 °C in this study. The isotopic composition of fluid inclusions is relatively easily changed at these temperatures, without opening (cracking) or deforming the inclusion walls. The fugacity gradients of both  $\text{H}_2\text{O}$  and  $\text{D}_2\text{O}$  are the only active driving forces in these re-equilibration experiments of fluid inclusions. Diffusion of fluid components through a solid quartz crystal, as interstitial particles or substitute particles, is the only process that is triggered by this gradient in our experiments, according to Fick's law. Several types of diffusion within quartz are described in the literature (see Bakker 2009 and reference therein). Diffusion of  $\text{H}_2\text{O}$

**Fig. 10**  $T_m(\text{ice})$  values versus relative size of fluid inclusions of the re-equilibration experiment *R004a* (a) at 600 °C and 19-day run-time and *R004c* (b) at 600 °C and 40 days run-time. Inclusions are selected at approximately 25 and 75  $\mu\text{m}$  depth in a, and at approximately 25 and 100  $\mu\text{m}$  depth in b. The dashed lines illustrate general trends in concentration dependent on inclusion size at constant depths



along dislocation lines (“pipe diffusion”) or other crystal defect structures is supposed to play an important role in re-equilibration experiment with additional pressure gradients that result in local deformation adjacent to fluid inclusions (e.g. Bakker and Jansen 1990, 1994; Audétat et al. 1999). This type of diffusion can be excluded in our experiments due to the absence of pressure gradients. Other types of diffusion can be summarized as bulk diffusion, which includes “self-diffusion” (e.g. Farver and Yund 1991) and “tracer-diffusion” (e.g. Kronenberg et al. 1986). It is assumed that bulk diffusion is the dominant process in our experiments. A variety of parameters that play a significant role in bulk diffusion processes are as follows: (1) gradient in chemical potentials of fluid components (i.e. concentration gradients) between inclusions and external pore fluids; (2) temperature and pressure; (3) experimental run-times; (4) distance of inclusions to crystal surfaces; and (5) inclusion size. These are exactly the parameters that are measured and defined in our experiments, consequently, our data can be used to calculate diffusion coefficients in a mathematical model as illustrated by Bakker (2009). Diffusion coefficients can be used to calculate concentration profiles of fluid components in quartz and fluid inclusions at variable temperatures and selected experimental run-times. Moreover, concentration profiles can be calculated at a geological time scale, because diffusion constants are time-independent.

The bulk diffusion model developed by Bakker (2009) is used to determine the diffusion coefficient of  $\text{H}_2\text{O}$  and  $\text{D}_2\text{O}$ . It is assumed that the solubility of  $\text{H}_2\text{O}$  and  $\text{D}_2\text{O}$  is similar in quartz (4.4  $\mu\text{mol}$  per Si), and both have similar diffusion coefficient. Furthermore, it is assumed that the fluid mixture of  $\text{H}_2\text{O}$  and  $\text{D}_2\text{O}$  in inclusions behaves like an ideal mixture at experimental condition, in order to be able to determine the individual fugacity coefficients of  $\text{H}_2\text{O}$  and  $\text{D}_2\text{O}$ . The geometry of our quartz crystal (short cylinder) differs from a spherical crystal in the model of

Bakker (2009); however, the use of a three-dimensional diffusion model is preferred in our approach, and the deviating geometries have only a minor effect on the estimated concentration profiles. Concentration profiles are calculated for a 5- $\mu\text{m}$ -diameter fluid inclusion after 1 and 19-day experimentation run-time at 600 °C and 337 MPa (Fig. 11a), by varying the diffusion coefficient until a similar profile is obtained as illustrated in Fig. 8a, c. The hypothetical concentration profiles in Fig. 11a are consistent with our experimental data by using a diffusion coefficient of about  $10^{-14} \text{ m}^2 \text{ s}^{-1}$ . Minor differences after 1 day of experimentation can be explained by the difference in  $\text{H}_2\text{O}$  and  $\text{D}_2\text{O}$  diffusion coefficients. Our experimental data evidence that  $\text{H}_2\text{O}$  is faster diffusing than  $\text{D}_2\text{O}$ , which is mainly noticeable in short run-time experiments (Fig. 5). After 19 days of experimentation, the concentration profile that is calculated with the same diffusion coefficient fits even better our experimental data and is not anymore affected by small difference in  $\text{H}_2\text{O}$  and  $\text{D}_2\text{O}$  diffusion coefficients. The value of the  $\text{H}_2\text{O}$  diffusion coefficient in our experiments is a factor 100 lower than the values estimated for hydrogen diffusion in the  $\beta$ -quartz field at higher temperatures and pressures (see Bakker 2009 and references therein).

The experimentally determined variable  $\text{D}_2\text{O}$  concentration in fluid inclusions at equal depth is mainly defined by fluid inclusions size: Small inclusions are richer in  $\text{D}_2\text{O}$  than large inclusions (Fig. 10). The fluid inclusion size parameter is tested with the bulk diffusion model that is used in the previous paragraph to estimate the diffusion coefficient. At 600 °C and 19-day experimentation run-time, the modeled  $\text{D}_2\text{O}$  concentration at 75  $\mu\text{m}$  and 50  $\mu\text{m}$  depth has a minor variation as a function of inclusion size, which confirms the observation that larger inclusions are less affected than smaller inclusions (Fig. 11b). However, the amount of change in  $\text{D}_2\text{O}$  content does not correspond to our observations (c.f. Fig. 11b, 10). The bulk diffusion



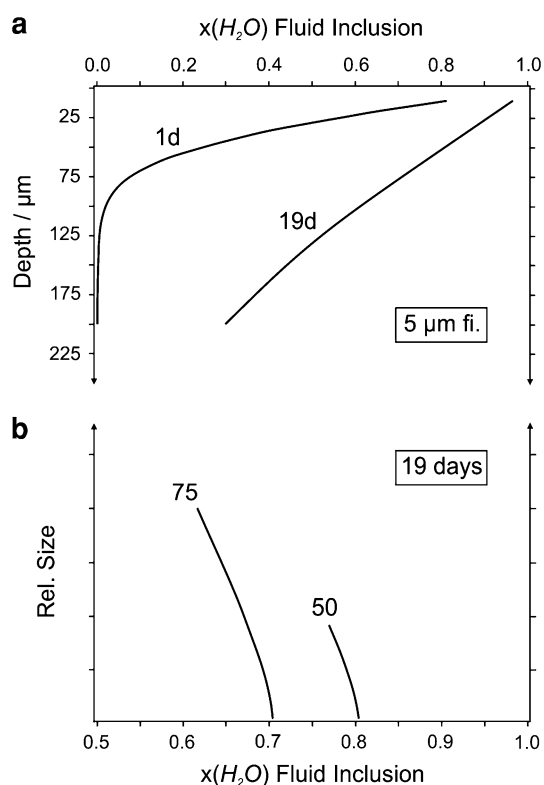


**Fig. 11** H<sub>2</sub>O concentration profiles calculated according to the bulk diffusion model of Bakker (2009). **a** for 5-μm-diameter fluid inclusions after 1 and 19 days of experimentation; **b** after 19 days of experimentation and variable inclusion sizes at 50 μm depth and 75 μm depth. (see text for further details)

model is based on specific boundary conditions, which include geometry definition, radial non-steady state diffusion, infinite external fluid source, solubility of H<sub>2</sub>O in quartz, and a distribution coefficient ( $K$ ) that defines the partitioning of D<sub>2</sub>O/H<sub>2</sub>O in quartz and fluid inclusions (see Appendix A in Bakker 2009). The  $K$  coefficient has a major impact on the calculation of D<sub>2</sub>O concentrations in fluid inclusions. The value of  $K$  was theoretically estimated (see Bakker 2009) and related to the partial molar volume of H<sub>2</sub>O in quartz. The  $K$  coefficient can also be related to fluid inclusion size, and preliminary calculations have indicated that concentration profiles as illustrated in Fig. 10 can be reproduced with the same diffusion coefficient that was estimated in the previous paragraph ( $10^{-14} \text{ m}^2 \text{ s}^{-1}$ ). Modeling of the  $K$  coefficient will be presented in following studies.

#### Natural fluid inclusions

The results of our study illustrate that fluid inclusions can be re-equilibrated in relatively short experimental run-times at elevated temperatures and pressures. The hydrogen isotope composition of fluid inclusions can be

adjusted instantaneously to external fluid conditions in a geological time scale. It is important to emphasize the differences between experimental work and processes that may occur in natural rock. Our experimental studies are focussed on the effect of one parameter, that is, fugacity gradient, and the experimental setup is designed to optimize processes that are induced by this gradient, whereas other parameters remain constant. The experiments have illustrated what a fugacity gradient can provoke in seemingly isolated fluid cavities within anhydrous crystals. In natural rock, the porosity is defining the existence of a fluid phase, and natural quartz grains are not completely surrounded by pore space with an infinite fluid source. The porosity decreases with increasing depth, therefore, sedimentary rocks have a larger fluid source than metamorphic and magmatic rocks. Size and shape of the pores, in addition to the network of pores, define the availability of the external fluid source in natural rock. Pores may cover 50 area % of the quartz surface in sedimentary rock and down to a few percentages (or less) in metamorphic rock. Diffusion of external fluids into quartz grains can only occur at pore–grain interfaces and will mainly effect those inclusions that are closer to this interface, whereas inclusions near grain–grain interfaces may not be effected. Otherwise, a threshold temperature of about 450 °C at 337 MPa is identified for diffusion processes in this study, which become more efficient at higher temperatures. In other words, sedimentary rocks have a large fluid source available, but temperatures may not reach values for efficient fluid inclusion re-equilibration, whereas metamorphic rocks contain sufficient heat but have low porosities. Nevertheless, interpretation of hydrogen isotope analyses of fluid inclusions in metamorphic and magmatic rocks must include the possibility of fluid inclusion re-equilibration.

#### Other re-equilibration experiments

The significance of fluid inclusion re-equilibration is already considered since the first knowledge on fluid inclusion properties (e.g. Brewster 1845). The first experimental evidence that fluid inclusions may be affected by changes in fluid density and the development of inclusion haloes is given by Lemlein (1956), Leroy (1979), and Pecher (1981). The processes that have been proposed in the literature to change the properties of fluid inclusions are as follows: (1) diffusion; (2) recrystallization; (3) stretching; (4) deformation; and (5) decrepitation. The driving forces of these processes are heat, concentration gradients, and pressure gradients. Re-equilibration studies of fluid inclusions are mainly performed with a pressure gradient, that is, a pressure difference between fluid inclusions and an external fluid pressure medium (e.g. Sterner and Bodnar

1989; Bakker and Jansen 1990; Vityk and Bodnar 1995). Occasionally, these experiments have been combined with a concentration gradient, that is, a gradient in chemical potentials between fluid components in fluid inclusions and the external fluid. The observed changes in fluid inclusions (i.e. shape, density, and composition) are defined by the sum of all these processes that are activated by these driving forces. However, the effect of individual processes cannot be quantified because these experiments include abundant independent and unrestrained parameters. For example, isothermal decompression of quartz samples with pure H<sub>2</sub>O fluid inclusions results in internal overpressures, which may cause stretching, deformation, and decrepitation (e.g. Sterner and Bodnar 1989). The decompression is also accompanied with a change in fugacities in the experimental capsule fluids, which may cause diffusion. Fugacity gradients are intensified if the composition of the capsule fluid is modified. Density and compositional changes of fluid inclusions are caused by these simultaneously operating processes, but it is not possible to identify the importance of individual processes in these experiments, and there is no unambiguous relationship between cause and result.

Sterner et al. (1995), Bakker and Diamond (2003), and Bakker (2007) provide the only examples of re-equilibration experiments at constant temperature and pressure with exclusively gradients in fluid component fugacities. The re-equilibration experiments in Sterner et al. (1995) are all performed within the  $\beta$ -quartz stability field at high temperatures and 300 MPa and short run-times (4 days). The lack of sufficient information and data presented, in addition to a number of inconsistencies, does not allow re-evaluation of these results. Bakker and Diamond (2003) and Bakker (2007) provided systematic studies on re-equilibration of fluid inclusions as a result of gradients in chemical potentials at constant pressure and temperature. A similar experimental setup is applied in the present study: The number of possible processes that may play a role in re-equilibration experiments is reduced and changes in fluid density and composition can be directly related to changes in homogenization and melting temperatures, due to the availability of accurate equations of the fluid state (H<sub>2</sub>O and D<sub>2</sub>O). Moreover, experimental conditions are within the  $\alpha$ -quartz stability field, to exclude any fluid inclusion changes that are induced by the  $\alpha$ – $\beta$  phase transition of quartz.

## Conclusions

Synthetic H<sub>2</sub>O-rich fluid inclusions in quartz have been re-equilibrated in a pure D<sub>2</sub>O pore fluid environment at 600 °C and 337 MPa. A gradient in fugacity is

superimposed in the experimental setup in order to provoke diffusion of H<sub>2</sub>O and D<sub>2</sub>O, whereas other parameters such as pressure gradient and deformation are excluded. In addition, experiments at 500, 400, and 300 °C with a constant pressure of about 337 MPa are performed to estimate the efficiency of temperature on diffusion processes.

The original synthesized fluid inclusions reveal only minor morphological changes, which are mainly determined by experimentation time. Re-equilibration experiments at 40 days reveal more equal to negative crystal shape inclusions than 1 or 5-day experiments. A total volume increase or decrease could not be detected in individual fluid inclusions.

The effect of diffusion through quartz is illustrated by the change in H<sub>2</sub>O–D<sub>2</sub>O composition of fluid inclusions at nearly equal densities. The D<sub>2</sub>O content in fluid inclusions is obtained from ice-melting temperatures, whereas changes in density are obtained from total homogenization temperatures.

At 600 °C and 337 MPa, 1- and 5-day re-equilibrations illustrate that H<sub>2</sub>O is faster diffusing out of inclusions than D<sub>2</sub>O is diffusing into inclusions. This process also results in a decrease in density of these inclusions. After 19- and 40-days re-equilibration, D<sub>2</sub>O concentration reaches values up to 63 mol %, whereas the density is restored to original values that correspond to the experimental temperature–pressure conditions.

The 19-day re-equilibration experiments are performed at 300, 400, 500, and 600 °C, and a constant pressure of 337 MPa. Maximum D<sub>2</sub>O concentration at 600 °C is about 63 mol %, whereas at 500 °C, values are obtained of maximally 27 mol %. D<sub>2</sub>O is not detected in fluid inclusions at 300 and 400 °C re-equilibration experiments.

Concentration profiles of D<sub>2</sub>O content within quartz are obtained from measured distances between inclusions and crystal surface. Shallow inclusions reach faster higher D<sub>2</sub>O concentrations than deep inclusions. However, a range of D<sub>2</sub>O concentrations is observed at equal depths, which is defined by the size of the inclusions. Small inclusions have higher D<sub>2</sub>O concentrations than large inclusions at equal depth. The concentration profiles are used to estimate a diffusion coefficient for D<sub>2</sub>O and H<sub>2</sub>O of about  $10^{-14} \text{ m}^2 \text{ s}^{-1}$  at 600 °C and 337 MPa, that is, with the  $\alpha$ -quartz stability field.

Natural fluid inclusions that are used to measure hydrogen isotopic compositions in order to identify fluid sources can be effected by diffusion processes, and pore fluid compositions may totally control inclusion compositions at high temperatures and pressure. The absence of pore fluids in metamorphic rock, and the relative low temperature and pressure conditions in sedimentary rock may prevent any diffusion processes.

**Acknowledgments** We would like to thank two anonymous reviewers, and the Austrian Research Fund (FWF) for financial support (project no. P 22446-N21).

## References

- Audétat A, Günther D (1999) Mobility and H<sub>2</sub>O loss from fluid inclusions in natural quartz crystals. *Contrib Mineral Petrol* 137:1–14
- Ayllón F, Bakker RJ, Warr LN (2003) Re-equilibration of fluid inclusions in diagenetic-anchizonal rocks of the Ciñera-Matallana coal basin (NW Spain). *Geofluids*
- Bakker RJ (2003) Package FLUIDS 1. Computer programs for analysis of fluid inclusion data and for modeling bulk fluid properties. *Chem Geol* 194:3–23
- Bakker RJ (2007) Diffusion of fluids through quartz. *Geochim Cosmochim Acta* 71:A54
- Bakker RJ (2009) Re-equilibration of fluid inclusions: bulk-diffusion. *Lithos* 112:277–288
- Bakker RJ, Diamond LW (2003) Fluid inclusion re-equilibration experiments in quartz: chemical potential gradients. *Acta Mineralogica-Petrographica, Abstract Series* 2:17–18
- Bakker RJ, Diamond LW (2006) Estimation of volume fractions of liquid and vapor phases in fluid inclusions, and definition of inclusion shapes. *Am Mineral* 91:635–657
- Bakker RJ, Jansen JBH (1990) Preferential water leakage from fluid inclusions by means of mobile dislocations. *Nature* 345:58–60
- Bakker RJ, Jansen JBH (1994) Raman Spectra of fluid and crystal mixtures in the systems H<sub>2</sub>O, H<sub>2</sub>O–NaCl and H<sub>2</sub>O–MgCl<sub>2</sub> at low temperatures: applications to fluid-inclusion research. *Can Miner* 42:1283–1314
- Bakker RJ, Baumgartner M, Doppler G (2012) Diffusion of water through quartz: a fluid inclusion study. *Goldschmidt 2012, Abstracts*
- Baumgartner M, Bakker RJ (2009) Raman spectroscopy of pure H<sub>2</sub>O and NaCl–H<sub>2</sub>O containing synthetic fluid inclusions in quartz—a study of polarization effects. *Mineral Petrol* 95(1–2):1–15
- Baumgartner M, Doppler G, Bakker RJ (2011) Preliminary results of experimental re-equilibration studies of natural H<sub>2</sub>O–CO<sub>2</sub>–NaCl-bearing fluid inclusions in quartz. *ECROFI-XXI, Abstracts*, pp 44–45
- Bodnar RJ, Sterner SM (1987) Synthetic fluid inclusions. In: Barnes HL, Ulmer GC (eds) *Hydrothermal experimental techniques*. Wiley, New York, pp 423–457
- Brewster (1845) On the modification of the doubly refracting and physical structure of topaz, by elastic forces emanating from minute cavities. *Philosophical Magazine Series* 3, V. 31, 206:101–104
- Crank J (1975) *The mathematics of diffusion*. Oxford science publications, Oxford
- Diamond LW, Tarantola A, Stünitz H (2010) Modification of fluid inclusions in quartz by deviatoric stress. II: experimentally induced changes in inclusion volume and composition. *Contrib Mineral Petrol* 160:845–864
- Dublyanski VD, Spötl C (2010) Evidence for a hypogene paleohydrogeological event at the prospective nuclear waste disposal site Yucca Mountain, Nevada, USA, revealed by the isotope composition of fluid-inclusion water. *Earth Planet Sci Lett* 289(3–4):583–594
- Farver JR, Yund RA (1991) Oxygen diffusion in quartz: dependence on temperature and water fugacity. *Chem Geol* 90:55–70
- Giuliani G, France-Lanord C, Zimmermann JL, Cheilletz A, Arboleda C, Charoy B, Coget P, Fontan F, Giard D (1997) Fluid composition,  $\delta D$  of channel H<sub>2</sub>O, and  $\delta^{18}O$  of lattice oxygen in beryls: genetic implications for Brazilian, Colombian, and Afghanistani Emerald deposits. *Int Geol Rev* 39(5):400–424
- Haar L, Gallagher JS, Kell GS (1984) *NBS/NRC steam tables*. Hemisphere Publishing Corporation, Washington
- Hill PG, MacMillan CRD, Lee V (1982) A fundamental equation of state for heavy water. *J Phys Chem Ref Data* 11(1):1–14
- Hosieni KR, Howald RA, Scanlon MW (1985) Thermodynamics of the lambda transition and the equation of state of quartz. *Am Mineral* 70:782–793
- Keppler H, Smyth JR (2006) Water in nominally anhydrous minerals. *Rev Mineral Geochem* 62:5–8
- Kerrick DM (1987) Cold-seal systems. In: Ulmer GC, Barnes HL (eds) *Hydrothermal experimental techniques*. Wiley, New York, pp 293–323
- Kronenberg AK, Kirby SH, Aines RD, Rossman GR (1986) Solubility and diffusional uptake of hydrogen in quartz at high water pressures: implications for hydrolytic weakening. *J Geophys Res Solid Earth* (1978–1986), 91:12723–12741
- Lemlein GG (1956) Formation of fluid inclusions and their use in geological thermometry. *Geochemistry* 6:630–642
- Leroy A (1979) Contribution to the evaluation of internal pressure in fluid inclusions when they decrepitate. *Bull Min* 102:583–593
- Pecher A (1981) Experimental decrepitation and re-equilibration of fluid inclusions in synthetic quartz. *Tectonophysics* 78(1–4): 567–583
- Roedder E (1984) Fluid Inclusions. *Min Soc Am Rev in Min* 12:644
- Rull F (2002) Structural investigation of water and aqueous solutions by Raman spectroscopy. *Pure Appl Chem* 74(10):1859–1870
- Shapiro SS, Wilk MB (1965) An analysis of variance for normality (complete samples). *Biometrika* 52:591–611
- Shepherd TJ, Rankin AH, Alderton DHM (1985) *A practical guide to fluid inclusion studies*. Blackie, Glasgow-London
- Sterner SM, Bodnar RJ (1989) Synthetic fluid inclusions. VII. Re-equilibration of fluid inclusions in quartz during laboratory simulated metamorphic burial and uplift. *J Metamorphic Geol* 7:243–260
- Sterner SM, Hall LD, Keppler H (1995) Compositional re-equilibration of fluid inclusions in quartz. *Contrib Mineral Petrol* 119:1–15
- Vityk MO, Bodnar RJ (1995) Textural evolution of synthetic fluid inclusions in quartz during re-equilibration, with applications to tectonic reconstruction. *Contrib Mineral Petrol* 121:309–323
- Wilkinson JJ (2001) Fluid inclusions in hydrothermal ore deposits. *Lithos* 55:229–272